Experimental and Numerical Studies on the Shear-Sliding Behavior of Clay Brick Masonries

F. Ferretti & C. Mazzotti
Department of Civil, Chemical, Environmental and Materials Engineering, University of Bologna, Viale Risorgimento 2, 40136 Bologna, Italy

A. Incerti
CIRI Buildings and Construction, University of Bologna, Via del Lazzaretto 15/5, 40131 Bologna, Italy

ABSTRACT: The identification of the shear strength parameters of masonry can be carried out through different experimental techniques, aimed at reproducing typical failure modes of masonry structural elements. The objective of this work is to characterize the shear-sliding behavior of brick masonry through the execution of triplet tests on three different masonry typologies. Series of triplet tests (EN 1052-3) were performed in displacement control on standard samples, constituted of clay bricks and lime-based mortar, arranged in a stacked bond. The experimental results were analyzed and compared among the different masonry typologies trying to correlate the shear strength parameters to the mechanical properties of the materials. Numerical simulations of the experimental tests were also carried out, adopting a simplified micro-modeling approach. The nonlinear numerical analyses allowed to properly interpret the experimental outcomes and they were compared with them in terms of failure load, post-peak behavior and specimen deformability, obtaining a good agreement.

1 INTRODUCTION

Brick masonry is characterized by the presence of horizontal and vertical mortar joints, which influence the shear behavior of the structural elements since they represent surfaces of weakness along which the failure can occur (Lourenço 1996, Rots 1997). The shear-sliding failure mode of masonry panels can be described by the Coulomb friction criterion. In this case, the local properties of the mortar-brick interface, such as the initial shear strength and the friction coefficient, are the most important parameters to be defined.

Experimental laboratory tests may be performed to study the shear-sliding behavior of masonry and to evaluate the mortar joint shear capacity. Different test methods were proposed in past researches, varying the geometry of the specimen, the loading arrangement and the boundary conditions (Drysdale et al. 1979, Stöckl et al. 1990, Riddington & Jukes 1994, Van der Pluijm 1999). Indeed, several aspects should be considered in the design of a shear test setup to ensure the reliability of the results (Riddington et al. 1997). First of all, normal and shear stress distributions should be uniform along the sliding mortar joint. Then, the failure should initiate far from the joint edges and should propagate quickly on the entire joint length. Finally, the presence of tensile stresses should be checked and possibly avoided.

Finite element analyses were also performed with the aim of identifying the most reliable test method by investigating peculiar aspects of the different methodologies and highlighting their advantages and disadvantages (Jukes & Riddington 2000, Popal & Lissel 2010).

A particular focus is here devoted to the triplet test, as proposed by the standard EN 1052-3. During the test, a constant axial compression is applied to the specimen, while a shear load is imposed to the central brick to produce its sliding. This test was found to be adequate to provide reliable results (Jukes & Riddington 2001, Vermeltfoort 2010). However, the main issues of this test are: (i) stress concentrations close to the loading points; (ii) presence of bending moment along the joint, which causes non-uniform stress distributions and could lead to undesired failures.

The objective of the present research is to study the shear-sliding behavior of three different masonry typologies through the execution of triplet tests. The tests were conducted in displacement control with the aim of characterizing both the Mohr-Coulomb failure criterion describing the masonry peak shear strength, and the post-peak behavior. Moreover, the transverse expansion upon shearing along the mortar joint, also known as dilatancy, was investigated. Indeed, it was found in previous researches (Van der Pluijm et al. 2000, Van Zijl 2004, Ferretti et al. 2018) that the dilatant behavior of masonry could af-

fect the test results, especially if it is restrained to some extent during the sliding process, e.g. due to the boundary conditions of the setup.

Numerical simulations of the experimental triplet tests were also carried out to better investigate the shear-sliding failure, through the analysis of the stress distributions along the mortar joint and the development of the cracking process.

2 MATERIALS AND METHODS

In the experimental campaign, series of triplet tests (EN 1052-3) were performed on standard samples, built with clay bricks and lime-based mortar, arranged in a stacked bond. Mortar joints were characterized by a thickness approximately equal to 10 mm. In particular, three masonry typologies were studied, differing in the mortar composition from one another. The main characteristics of the triplet samples are presented in Table 1, while the mechanical characterization of the constituent materials is described in the following Sections.

Table 1. Characteristics of the triplet samples.

Triplet Series	Brick Type	Mortar Type	Nr. Specimens	Dimensions (mm^3)
A-M1	IBL_BN	M1	4	250×170×120
B-M2	IBL_BN	M2	4	250×170×120
C-M3	IBL_BN	M3	4	250×170×120

2.1 *Bricks*

The brick elements chosen for the construction of the triplet samples were handmade fired clay bricks, whose dimensions are reported in Table 2. Cylindrical specimens, characterized by a height-to-diameter ratio h/d equal to 1, were cored from the bricks and tested in compression for their mechanical characterization. The mean brick compressive strength $f_{b,c}$, together with the brick density γ_b, is reported in Table 2.

Table 2. Mechanical properties of the bricks.

Brick	l_b (mm)	w_b (mm)	h_b (mm)	γ_b (kg/m^3)	$f_{b,c}$ (MPa)	CoV (%)
IBL_BN	250	120	50	1640	22.4	15.8

2.2 *Mortars*

In the experimental campaign, three different natural hydraulic lime-based mortars (NHL) were adopted. Starting from a pre-mixed mortar available on the market, three different mix designs were prepared to obtain low strength mortars but with an adequate workability. In more detail, different growing water/binder ratios w/b were considered to reduce the mortar strength. In parallel, given the significant water content, the amount of fine sand (s), was increased to ensure the mix workability. Characteristics of mortar mixes are presented in Table 3, where proportions (b:w:s) are referred to weights.

Standard laboratory tests, such as monotonic uniaxial compression tests and three-point bending tests (EN 1015-11), were conducted to determine the mortar compressive strength $f_{m,c}$ and the mortar flexural strength $f_{m,fl}$. Results are reported in Table 4 and refer to mortars cured in laboratory conditions (T=22°±1°, RH=50%±5%) for 60 days.

Table 3. Mortar mix designs.

Mortar Type	Mix Design	w/b	$w/(b+s)$	s/b	w/tot
M1	1:1.4:4.7	1.4	0.25	4.7	0.20
M2	1:1.4:6.1	1.4	0.20	6.1	0.17
M3	1:1.7:7.6	1.7	0.20	7.6	0.17

Table 4. Mechanical properties of mortars.

Mortar	$f_{m,c}$ (MPa)	CoV (%)	$f_{m,fl}$ (MPa)	CoV (%)
M1	4.10	4.4	1.30	5.1
M2	3.52	2.7	1.26	0.5
M3	2.67	2.2	0.88	7.5

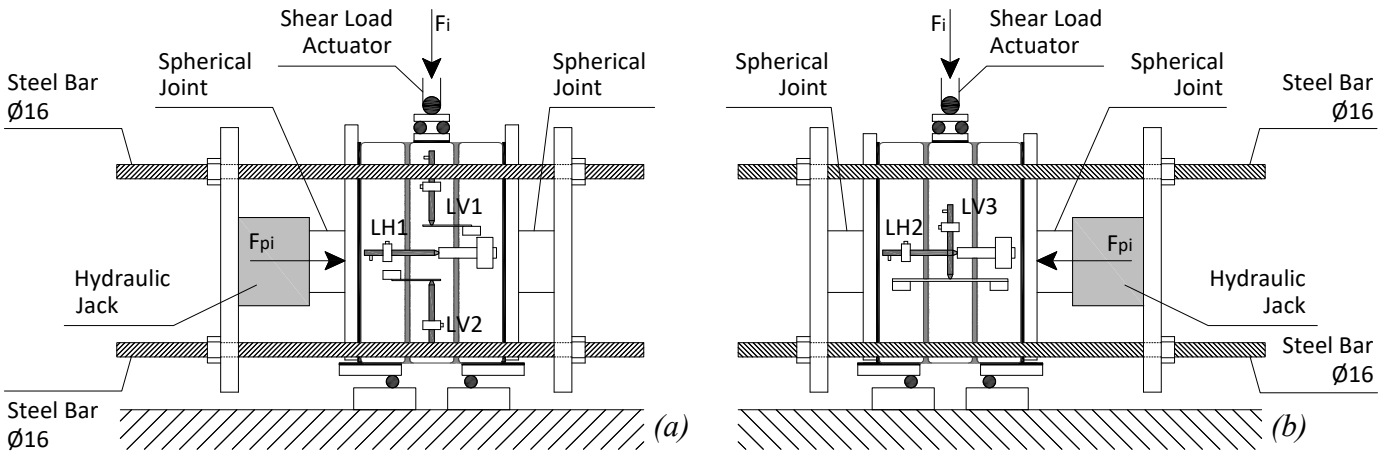

Figure 1. Triplet test setup and instrumentation on (a) side *A* and (b) side *B*.

2.3 *Triplet Test*

In the triplet test, according to the EN1052-3 Standard, a prescribed level of axial compression can be applied to the masonry samples, orthogonally to the mortar joints. Then, a monotonically increasing shear load is imposed to the central brick to produce its sliding. The possible failure modes can be distinguished as: (i) *Type A*, failure at the mortar-to-brick interface; (ii) *Type B*, failure within the mortar joints; (iii) *Type C*, failure within the brick element, and (iv) *Type D*, diagonal failure of the triplet specimen.

In the experimental campaign, a test setup (Fig. 1) was purposely designed for the execution of the triplet tests, allowing for the application of the shear load F_i in displacement control, by using a servo-hydraulic machine, with a maximum capacity of 100 kN (load cell class 0.5). Before the application of the shear displacement, a uniform lateral compression force F_{pi} was applied to the samples, orthogonal to the bed joints, through a hydraulic jack with a maximum capacity of 750 kN. The jack was controlled by an electric pump, allowing to maintain a constant pre-compression level throughout the test.

The system adopted for the application of the axial compression force F_{pi} was a closed system constituted by four threaded steel bars (∅16) and four steel plates. In particular, the steel plates in contact with the lateral surface of the bricks were characterized by a thickness of 15 mm, while the external steel plates were 20 mm thick. Spherical joints were inserted between the hydraulic jack and the internal steel plate, on one side, and between the two steel plates, on the other side, to allow the specimen to rotate, avoiding the occurrence of parasitic stresses which could influence the uniformity of the compressive stress distribution along the mortar joints. Neoprene pads were interposed between the bricks and the steel plates.

For each masonry typology, the following axial compression levels were considered: 0.10, 0.20, 0.60, 1.00 MPa. The shear displacement rate was equal to 1.20 mm/min. In some cases, after the onset and development of the sliding failure, the precompression level was increased and the sliding was produced again, as will be explained in the following.

Linear Variable Differential Transformers (LVDT) were used, on both sides of the triplet samples, to monitor the displacements during the tests. In particular, the relative vertical displacements between the central brick and the lateral ones (shear displacements v) were measured by means of three vertical LVDTs, while the expansion upon shearing due to dilatancy (normal displacement u) was measured by means of two horizontal LVDTs positioned in the center of the specimens (Fig. 1).

3 EXPERIMENTAL RESULTS OF THE TRIPLET TESTS

The results of the triplet tests can be interpreted by considering the Mohr-Coulomb failure criterion, which is suitable to describe a shear-sliding failure mode. The criterion is considered here adequate since most of the samples failed with a *Type A* failure mode, characterized by the sliding along the mortar-to-brick interface (Fig. 2).

Figure 2. Typical failure modes of the triplet tests (*Type A*): (a) pure sliding along the brick-to-mortar interface; (b) sliding with mortar crushing at the joint extremities.

Typical shear stress τ *vs* shear displacement v_{mean} curves are plotted in Figure 3*a* for the specimen series A-M1. Four curves are reported, one for each axial compression level considered. From the graphs it is possible to notice that the initial branch is characterized by a significant stiffness and it can be considered linear up to the peak load. Only in one case (A-M1-4) a stiffness degradation is visible approaching the peak load, probably due to the formation of some micro-cracks, corresponding to a shear stress equal to 0.59 MPa. After the peak load, the quasi-brittle behavior of the shear sliding failure can be recognized with a softening branch and a residual horizontal plateau, corresponding to a dry friction condition (Van der Plujim et al. 2000). It is worth noticing that the failure brittleness decreases as the axial compression level increases. In general, the expected trend, i.e. higher shear strengths in correspondence with higher axial compressive stresses, was confirmed by the experimental results. The presence of two peak loads, such as for the triplet specimens A-M1-2 and A-M1-3, indicates the non-simultaneous failure of the two mortar joints, thus the non-symmetric behavior of the samples, due to intrinsic differences within the mortar or to the construction process of the samples.

Focusing on the dilatant behavior of the samples, in Figure 3*b* the normal displacement u_{mean} *vs* shear displacement v_{mean} diagrams are reported for the specimen series A-M1. Positive normal displacements indicate a lateral expansion of the sample. It is clearly noticeable that the expansion upon shearing,

due to dilatancy, is the highest for the specimen subject to an axial compressive stress equal to 0.1 MPa, while it is lower, but still positive, for the triplet sample tested with an axial compression level of 0.2 MPa. The normal displacement tends to zero or even becomes negative for higher compressive stresses. In this latter case, a lateral contraction of the specimens is registered during the sliding failure, which can be related to the crumbling or crushing of the mortar in compression. This phenomenon was indeed prevalent for specimens built with the weakest mortars.

The trends here described for the specimen series A-M1 were also observed for the series B-M2 and C-M3, here not fully reported for sake of brevity.

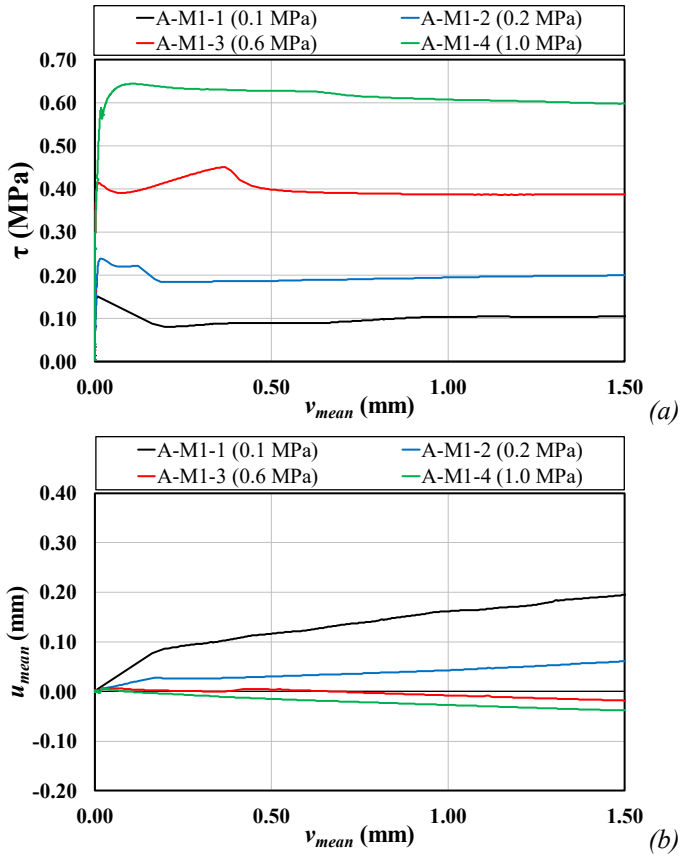

Figure 3. Triplet test results for the specimen series A-M1: (a) shear stress τ *vs* shear displacement v_{mean} diagram; (b) normal displacement u_{mean} *vs* shear displacement v_{mean} diagram.

As a result of each triplet test, the stress state (σ; τ) in correspondence of the peak load and in the post peak phase (v_{mean}=1.50 mm) has been measured and reported in Table 5. In particular, for those samples subject to the axial stress increase, after the development of the first sliding, more than one residual stress state was determined. Starting from these results, it was possible to calibrate a Mohr-Coulomb failure criterion for each masonry typology, according to Equation 1:

$$\tau = f_{v0} + \sigma \tan\varphi, \quad (1)$$

where f_{v0} is the shear strength at zero compressive stress, i.e. cohesion or initial shear strength, and φ is the friction angle. In a similar way, a residual failure criterion (Van der Pluijm et al. 2000), characterized by a residual shear strength $f_{v0,res}$ and by a residual friction angle φ_{res}, can be determined by plotting the residual stress τ_{res} *vs* the corresponding compressive stress σ and performing a linear interpolation.

Table 5. Triplet test results: stress state at the peak load and in the residual phase.

Specimen Code	σ (MPa)	τ_u (MPa)	τ_{res} (MPa)
A-M1-1	0.10	0.15	0.09
A-M1-1*	0.38	-	0.27
A-M1-2	0.20	0.24	0.20
A-M1-3	0.62	0.45	0.39
A-M1-3*	1.03	-	0.62
A-M1-4	1.02	0.64	0.58
B-M2-1	0.10	0.14	0.08
B-M2-2	0.21	0.20	0.14
B-M2-3	0.61	0.42	0.39
B-M2-3*	1.02	-	0.60
B-M2-4	1.02	0.64	0.63
C-M3-1	0.11	0.14	0.08
C-M3-1*	0.61	-	0.40
C-M3-1**	1.02	-	0.63
C-M3-2	0.20	0.18	0.14
C-M3-2*	0.65	-	0.39
C-M3-2**	1.02	-	0.51
C-M3-3	0.62	0.38	0.34
C-M3-3*	1.02	-	0.55
C-M3-4	1.02	0.59	-

*,** further reloading phases

Table 6. Triplet test results: shear strength parameters.

Specimen Code	f_{v0} (MPa)	tanφ (-)	$f_{v0,res}$ (MPa)	tanφ_{res} (-)
A-M1	0.12	0.52	0.06	0.53
B-M2	0.09	0.54	0.02	0.59
C-M3	0.08	0.49	0.04	0.52

The shear strength parameters obtained from the elaboration of the experimental results are reported in Table 6, for both the peak and the residual Mohr-Coulomb failure criteria, which are plotted in Figures 4*a-b*, respectively. The values of the cohesion f_{v0} can be directly correlated to the mortar properties: the lower the compressive or flexural strength of the mortar, the lower the cohesion. Considering the friction coefficient (tanφ), a clear correlation cannot be found with the mortar strength. Nevertheless, it can be observed that for the specimens built with mortars characterized by the same water binder ratio (M1 and M2), a higher value of the friction coefficient was obtained for the series having the greater amount of fine sand (M2). The friction coefficient can be indeed more related to the mortar composition and to the brick surface characteristics, rather than to the mortar mechanical properties, given the

failure mode observed in the present experimental tests. The values of the residual shear strength $f_{v0,res}$, theoretically equal to zero, are quite low and significantly lower than the corresponding values of f_{v0}. A slight friction hardening in the post-peak phase is noticeable for all the specimen series.

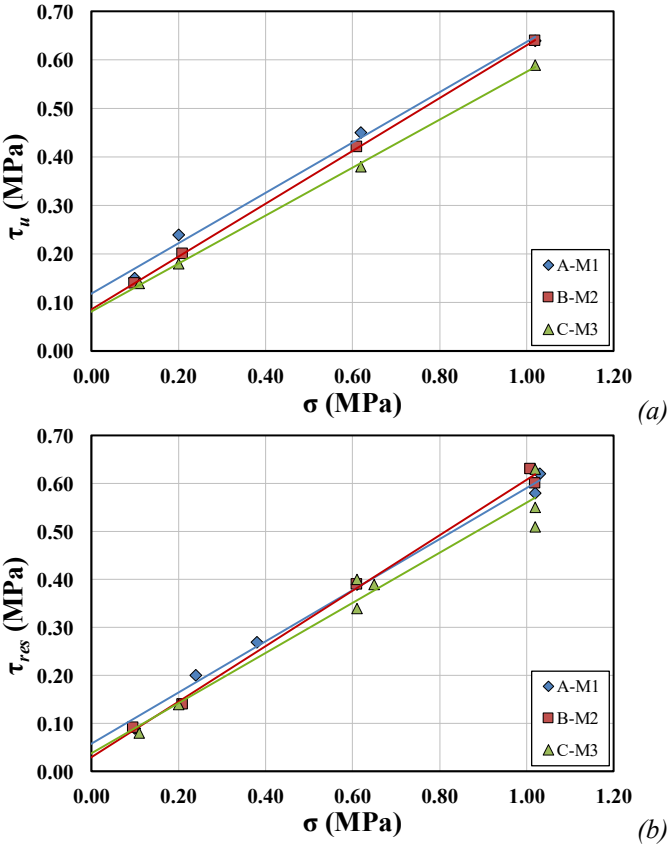

Figure 4. Determination of Mohr-Coulomb failure criteria: (a) peak shear stress τ_u *vs* compressive stress σ diagram; (b) residual shear stress τ_{res} *vs* compressive stress σ diagram.

4 NUMERICAL ANALYSES

4.1 *Numerical model*

Modeling of masonry structures can be performed according to different approaches, i.e. macro-modeling or micro-modeling approaches, depending on the desired level of accuracy (Lourenço et al. 1995, Rots 1997). It is, indeed, possible to model masonry as a composite or to singularly model its constituents. In the numerical analyses here presented, a micro-modeling approach was chosen, given the level of accuracy needed to study the sliding failure along the mortar joint and considering the limited dimensions of the triplet samples. In more detail, a simplified micro-modeling strategy was adopted, which implies to model the mortar joints as zero thickness interface elements and the bricks as continuum element characterized by an expanded geometry to maintain the overall dimensions of the sample unchanged.

A 2D model was adopted for the numerical simulations of the triplet test and, due to the symmetry of the test setup, only half of the specimen was considered. The details of the mesh used in the numerical models are shown in Figure 5. Bricks were modeled using quadratic 8-noded plane stress elements, while line 3-noded interface elements were adopted to model the zero-thickness mortar joint. The steel plates in contact with the sample were also modeled with quadratic 8-noded plane stress elements and interface elements were inserted between the steel elements and the bricks. A linear elastic behavior was considered for bricks and steel, while nonlinearities were only assigned to the interface elements.

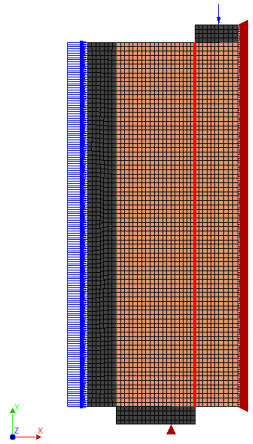

Figure 5. Finite element model.

To describe the behavior of interface elements in the linear elastic range, it is necessary to define the normal and shear stiffness parameters, k_n and k_t. In particular, for the interface elements adopted to model the mortar joint, the approach proposed by Rots (1997) was considered and the stiffness parameters were determined through Equations 2 and 3:

$$k_n = \frac{E_b E_m}{t_m (E_b - E_m)} \tag{2}$$

$$k_t = \frac{G_b G_m}{t_m (G_b - G_m)} , \tag{3}$$

where E_b and G_b are the elastic and shear modulus of the bricks, E_m and G_m are the elastic and shear modulus of the mortar, and t_m is the mortar joint thickness. For the interface elements adopted to model the brick-to-plate contact surfaces, the normal and shear stiffness coefficients were calibrated to allow the transfer of compressive stresses and to avoid the lateral confinement of the bricks, thus a dummy value was given to the normal stiffness coefficient k_n and a very low value was assigned to the shear stiffness coefficient k_t.

The nonlinear behavior along the mortar sliding interface was described with a composite interface

model, including a Coulomb friction criterion, a tension cut-off and a compressive cap (Lourenço 1996). Exponential softening for tension and shear failure modes were included, while a hardening/softening behavior was considered in compression. The interface elements between the steel plates and the bricks were considered as a no-tension material.

With reference to the Coulomb friction model, the yielding function is expressed as:

$$f\left(\sigma,\kappa_2\right)=\left|\tau\right|+\sigma\tan\varphi(\kappa_2)-f_{v0}(\kappa_2)\,, \tag{4}$$

where κ_2 is a scalar indicating the amount of softening, assumed equal to the plastic shear displacement. In Equation 4, cohesion and friction softening are introduced: an exponential softening for the cohesion, depending on the mode-II fracture energy G_f^{II}, and a friction softening, considered proportional to the cohesion softening, depending on the values of the initial and residual friction angles.

A non-associated plastic potential with a variable dilatancy angle ψ is considered, according to Equations 5 and 6 (Van Zijl 2004):

$$g_2=\left|\tau\right|+\sigma\tan\psi-f_{v0}\,, \tag{5}$$

$$\tan\psi=\tan\psi_0\left\langle 1-\frac{\sigma}{\sigma_u}\right\rangle e^{-\delta v_p}\,, \tag{6}$$

where v_p is the plastic shear displacement along the mortar joints, ψ_0 is the dilatancy angle at zero confining stress and shear slip, σ_u is the pre-compression level at which the dilatancy goes to zero, and δ is the dilatancy shear-slip degradation coefficient. It was demonstrated that the dilatancy is arrested under conditions of high axial compressive stress level and large plastic shear displacement (Van der Pluijm et al. 2000, Van Zijl 2004). These parameters can be calibrated if the expansion upon shearing is measured during the triplet tests, as done in the present experimental campaign, where the specimens were free to expand laterally.

Numerical simulations were performed with the finite element software DIANA FEA (Release 10.3) for the triplet series B-M2, at 4 different axial compression levels (0.10 – 0.20 – 0.60 – 1.00 MPa), to reproduce the loading conditions of the experimental tests. After the application of the lateral compressive distributed load, an increasing vertical displacement was imposed to the top plate. Regular Newton-Raphson method was adopted to solve the nonlinear problem.

The input parameters used in the numerical simulations are reported in Table 7. In particular, the parameters for the Coulomb friction model were calibrated from the experimental results of the triplet tests. The tensile strength and the mode-I fracture energy were determined as a fraction of the initial shear strength and the mode-II fracture energy, respectively (Rots 1997). The compressive strength f_c was evaluated using the formula provided by Eurocode 6, starting from the mechanical properties of the components. The compressive fracture energy was calibrated based on indications found in the literature and on previous experimental results on similar masonry typologies (Lourenço 1996, Rots 1997).

Table 7. Input mechanical parameters.

Parameter	Symbol	Units	Value
Elastic modulus of brick	E_b	(MPa)	5800
Poisson's ratio of brick	ν_b	(-)	0.20
Elastic modulus of mortar	E_m	(MPa)	3500
Poisson's ratio of mortar	ν_m	(-)	0.20
Elastic modulus of steel	E_s	(MPa)	210000
Poisson's ratio of steel	ν_s	(-)	0.30
Interface normal stiffness	k_n	(N/mm^3)	882.6
Interface shear stiffness	k_t	(N/mm^3)	367.8
Tensile strength	f_t	(MPa)	0.06
Mode-I fracture energy	G_f^I	(N/mm)	0.01
Cohesion	c_0	(MPa)	0.09
Friction angle	ϕ_0	(rad)	0.483
Residual friction angle	ϕ_{res}	(rad)	0.535
Dilatancy angle	ψ_0	(rad)	0.381
Confining normal stress	σ_u	(MPa)	0.50
Exp. degradation coeff.	δ	(-)	1.5
Mode-II fracture energy	G_f^{II}	(N/mm)	0.02
Compressive strength	f_c	(MPa)	7.07
Compr. fracture energy	G_f^c	(N/mm)	20

4.2 *Numerical results*

In this section, the results of the numerical simulations are presented and compared with the experimental results for the triplet series B-M2. In more detail, the comparisons are reported in Figure 6 in terms of shear stress τ *vs* shear displacement v_{mean} diagram (Fig. 6*a*) and normal displacement u_{mean} *vs* shear displacement v_{mean} diagram (Fig. 6*b*), for each axial compression level chosen.

With reference to Figure 6*a*, it can be noticed that the numerical models can properly capture the experimental behavior, especially in terms of peak shear stress. A good agreement is also noticed in the initial phase, up to the peak load, for triplets subject to axial compression stresses equal to 0.10, 0.20 and 0.60 MPa, while for the highest axial compression level (1.00 MPa) it can be observed that the numerical model cannot adequately describe the stiffness degradation approaching the peak load. In terms of residual shear stress, a slight underestimation is visible for all the axial compression levels. This can be explained by considering that the residual Mohr-Coulomb failure criterion was calibrated by using also the results obtained in the reloading phases, after the development of the first sliding failure.

Figure 6*b* shows a very good agreement between numerical and experimental results for axial com-

pression levels equal to 0.10 and 0.20 MPa, while for axial compression levels of 0.60 and 1.00 MPa, the experimental curves show a compression orthogonal to the bed joint which is not well captured by the numerical results. This can be explained by considering some aspects related to the test setup – e.g. specimens not completely free to expand laterally at high axial compression stress levels – or by considering that the failure mode observed in these experimental tests, especially for the axial compression stress of 1.00 MPa, was not a pure sliding failure along the brick-mortar interface but involved the mortar also, as visible in Figure 2*b*. Indeed, cracking in the mortar occurred, especially closed to the joint edges. In order to capture the very low – even negative – values of normal displacements u_{mean}, a detailed micro-modeling strategy, not reported in this work, should be adopted.

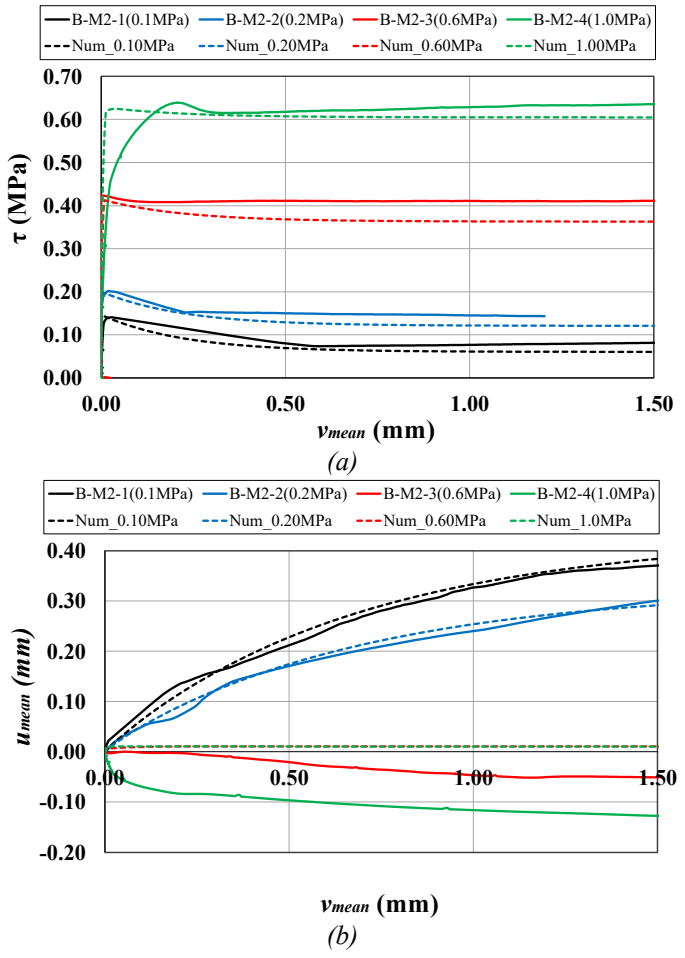

Figure 6. Experimental *vs* numerical results for the specimen series B-M2: (a) shear stress τ *vs* shear displacement v_{mean} diagram; (b) normal displacement u_{mean} *vs* shear displacement v_{mean} diagram.

Considering the results of the nonlinear analyses, it is interesting to investigate the development of the stress distributions along the joint and the propagation of the failure, given that they could influence the reliability of the results.

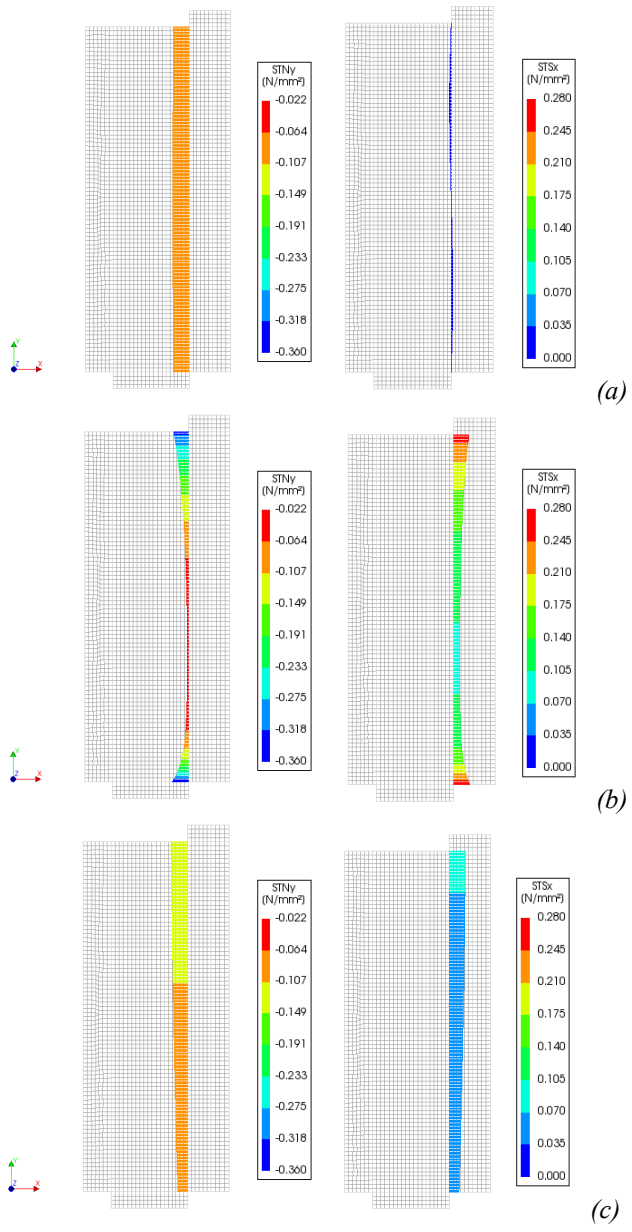

Figure 7. Normal and tangential stress distributions along the sliding mortar joint: (a) application of the axial compressive stress; (b) peak load; (c) shear displacement equal to 1.00 mm – residual phase.

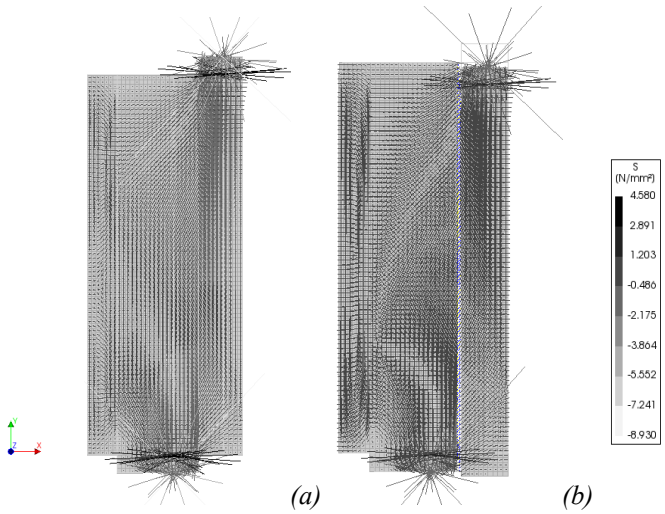

Figure 8. Principal stress distribution: (a) peak load; (b) shear displacement equal to 1.00 mm – residual phase.

In Figure 7, the evolution of the normal and tangential stresses along the sliding interface are shown, for an initial axial compression level equal to 0.10 MPa. It can be noticed that: (i) at the beginning of the test, the normal stress is uniform along the interface, while the tangential stress is negligible; (ii) at the peak, the stress distributions are not uniform along the joint, with concentrations of stresses occurring at the joint edges; (iii) in the residual pure frictional phase, the stress distributions tend to be more uniform along the joint, slightly higher in the upper portion of the specimen. The principal stress distributions for an axial compression level equal to 0.1 MPa are reported in Figure 8, where stress concentrations close to the loading plates are clearly visible, together with the presence of a compressed strut developing within the triplet specimen across the sliding mortar joint. Worth mentioning that the failure started from the joint extremities but then propagated quickly along the entire interface.

5 CONCLUSIONS

The objective of the research was to analyze the shear-sliding behavior of three brick masonry typologies, built using different mortar mixes, through the execution of triplet tests. Numerical simulations of the tests were also carried out considering the mechanical parameters obtained or calibrated from the experimental results.

The experimental tests were performed in displacement control, allowing to evaluate the peak shear strength of masonry and to analyze the post-peak nonlinear behavior. Mohr-Coulomb failure criteria were calibrated for the investigated masonry typologies, both at the peak and in the residual phase. The obtained mechanical properties were compared with the characteristics of the mortar used for the construction of the specimens and a correlation was found between the initial shear strength and the mortar compressive and flexural strength, i.e. the lower the mechanical properties of the mortar, the lower the initial shear strength. Therefore, it is worth highlighting that the mortar composition can affect the sliding-shear strength of masonry and the quality of the bond along the brick-mortar interface. In the experimental tests, a particular focus was also devoted to the investigation of the dilatant behavior of masonry through the measurements of the lateral expansion of the triplet sample upon shearing. The triplet specimen was, indeed, free to expand laterally during the test.

The numerical analyses allowed to better understand the onset and development of the sliding failure together with the evolution of the normal and tangential stress distributions along the mortar joint. Stress concentrations were noticed at locations corresponding to the joint edges, close to the loading plates. This observation can explain why mortar crushing was noticed at the joint extremities for few triplet samples. In general, it can be concluded that a good agreement was obtained between numerical and experimental results, confirming the suitability of the chosen modeling approach.

ACKNOWLEDGMENTS

This paper was supported by the PRIN 2017 research programme of the Italian Ministry of Education, University and Research, project DETECT-AGING, grant N. 201747Y73L.

REFERENCES

Drysdale, R.G., Vanderkeyl, R. & Hamid, A.A. 1979. Shear strength of brick masonry joints. *Proc. 5th Int. Brick and Block Mas. Conf., Washington D.C., 5-10 October 1979*.

Ferretti, F., Esposito, R., Rots, J.G. & Mazzotti, C. 2018. Shear-sliding behavior of masonry: numerical micro-modeling of triplet tests. *Proc. EURO-C Conf.*, *Austria, 26 February – 01 March 2018*.

Jukes, P. & Riddington, J.R. 2000. Finite element prediction of block triplet shear strength. *Proc. 12th Int. Brick and Block Mas. Conf., Madrid, 25-28 June 2000*.

Jukes, P. & Riddington, J.R. 2001. The failure of brick triplet test specimens. *Masonry International*, 15(1).

Lourenço, P.B., Rots, J.G. & Blaauwendraad, J. 1995. Two approaches for the analysis of masonry structures: micro and macro-modeling. *Heron*, 40(4):313-340.

Lourenço, P.B. 1996. Computational strategies for masonry structures, PhD thesis, Delft University of Technology.

Popal, R. & Lissel, S.L. 2010. Numerical evaluation of existing mortar joint shear tests and a new test method. *Proc. 8th International Masonry Conference, Dresden, 2010*.

Riddington, J.R., Fong, K.H. & Jukes, P. 1997. Numerical study of failure initiation in different joint shear tests. *Masonry International*, 11(2).

Riddington, J.R. & Jukes, P. 1994. A masonry joint shear strength test method. *Proc. Instn Civ. Engrs Structs & Bldgs*, 104:267-274.

Rots, J.G. 1997. *Structural Masonry – An experimental/numerical basis for practical design rules*, Rotterdam: Balkema.

Stöckl, S., Hofmann, P. & Mainz, J. 1990. A comparative finite element evaluation of mortar joint shear tests. *Masonry International*, 3(3).

Van der Pluijm, R. 1999 Out of plane bending of masonry. *Ph.D. Thesis. Eindhoven University of Technology, The Netherlands.*

Van der Pluijm, R., Rutten, H. & Ceelen, M. 2000. Shear behaviour of bed joints. *Proc. 12th Int. Brick and Block Mas. Conf., Madrid, 25-28 June 2000*.

Van Zijl, G. 2004. Modeling masonry shear-compression: role of dilatancy highlighted. *Journal of Engineering Mechanics*, 130(11):1289-1296.

Vermeltfoort, A.T. Variation in shear properties of masonry. *Proc. 8th International Masonry Conference, Dresden, 2010*.